PAPER

Raman quantum memory based on an ensemble of silicon-vacancy centers in diamond

IOP Publishing | Astro Ltd Laser Physics

Laser Phys. **29** (2019) 104001 (5pp) https://doi.org/10.1088/1555-6611/ab4049

Raman quantum memory based on an ensemble of silicon-vacancy centers in diamond

A Kalachev[1,2], A Berezhnoi[1], P Hemmer[1,3] and O Kocharovskaya[4]

[1] Zavoisky Physical-Technical Institute, FRC Kazan Scientific Center, Russian Academy of Sciences, 10/7 Sibirsky Tract, Kazan 420029, Russia
[2] Kazan Federal University, 18 Kremlyovskaya Str., Kazan 420008, Russia
[3] Department of Electrical and Computer Engineering, Texas A&M University, College Station, TX 77843-3128, United States of America
[4] Department of Physics and Astronomy and Institute for Quantum Science and Engineering, Texas A&M University, College Station, TX 77843-4242, United States of America

E-mail: a.a.kalachev@mail.ru

Received 1 September 2019
Accepted for publication 1 September 2019
Published 18 September 2019

Abstract

The possibility of implementing a cavity-enhanced off-resonant Raman quantum memory in an ensemble of silicon-vacancy centers in diamond is studied. It is shown that the signal-to-noise ratio at the output of the memory can significantly exceed unity for short single-photon pulses if the number of optical centers is small enough, which can be achieved with diamond samples in optical microresonators, and level splitting in their ground state is significantly enhanced by strain.

Keywords: quantum memory, silicon-vacancy center, diamond, Raman absorption, single photon, cavity, signal-to-noise ratio

(Some figures may appear in colour only in the online journal)

1. Introduction

Quantum memories are of crucial importance for developing quantum information technologies and form a platform for building scalable linear optical quantum computers, realizing long-distance quantum communications, etc (see [1, 2] for a recent review). At present, main attention is paid to quantum memory schemes utilizing the interaction of weak light pulses with ensembles of optical centers. These schemes are based on photon echo, electromagnetically induced transparency and off-resonant Raman absorption and emission of light pulses, making it possible to implement multimode quantum memory necessary for practical applications. As for the quantum information carriers, one of the promising materials for storage is diamond with color centers (see, e.g. [3, 4]). In particular, the negatively-charged silicon-vacancy centers (SiV^-) have recently attracted great attention [5–11] since they demonstrate large Debye–Waller factor, spectral stability, and a narrow inhomogeneous broadening of optical transitions. The latter makes these crystals promising candidates for implementing various memory protocols based on off-resonant Raman interaction [12–20]. Recently, an ensemble of nitrogen-vacancy centers has been considered in this context [21]. In particular, it was shown that a Λ-scheme with orthogonal linearly polarised optical transitions can be implemented in this system by application of external electric and magnetic fields, thereby minimizing four-wave mixing noise. However, large inhomogeneous broadening of optical transitions (typically tens of GHz), in addition to strong spectral diffusion ($\sim$100 MHz), is a significant problem. In the present work, we analyze the possibility of implementing optical quantum memory via off-resonant Raman absorption and emission of single-photon pulses in an ensemble of silicon-vacancy centers placed in a cavity and achieving large signal-to-noise ratio at the output of the memory device.

2. The model

The general scheme of quantum memory based on the Raman interaction of two fields with an ensemble of $N \gg 1$ color centers placed in a resonator is shown in figure 1(a). In the absence of an external magnetic field and strain, the SiV centers demonstrate an electronic level structure consisting of the ground-state and excited-state manifolds, each containing two branches with the frequency splitting of $\Delta_{GS} = 48$ GHz in the ground and $\Delta_{ES} = 259$ GHz in the excited state (see figure 1(b)). We assume that [1 1 1] axis of the color centers is oriented along the axis z perpendicular to the cavity axis. A weak signal field to be stored is supposed to act on the transition $|1\rangle - |3\rangle$ and polarized along the axis z, while the control field acts on the transition $|2\rangle - |3\rangle$ and polarized perpendicular to the [1 1 1] axis (y-polarized). In general case, the dipole moments of the optical transitions forming the Λ-scheme are not orthogonal so that the control field with frequency ω_c acts on both optical transitions, producing a Raman combination not only with the signal field (frequency ω_s) but also with an idler field (frequency ω_i). This results in an unwanted four-wave mixing process and corresponding noise that can prevent the implementation of Raman quantum memories (see [22] and references therein). It should be noted that without an external magnetic field each of the energy levels is doubly degenerate so that each of the Λ-schemes actually consists of two equivalent spin-preserving ones [23, 24]. In addition, similar Λ-schemes are formed with the upper state $|4\rangle$, which should be also taken into account in the numerical simulations.

The energy levels can be widely tuned in frequency by strain, which proves to be useful for several reasons. First, coherence time for the storage transition $|1\rangle - |2\rangle$ is increased up to 250 ns at liquid Helium temperature [25]. Second, increasing frequency splitting between the levels $|1\rangle$ and $|2\rangle$ makes it possible to store shorter single-photon pulses. Third, it allows one to use a frequency selective mirror in the resonator, thereby making linewidth for the control field broader than that for the signal field, which is necessary for optimal coupling by control field pulse shaping. In addition, as will be shown below, the larger the strain, the smaller the coupling of the control field to the unwanted transition in the Λ-scheme, which allows one to reduce noise at the output of the memory device.

3. Basic equations

To consider the cavity-assisted quantum memory, we take advantage of a theoretical model developed in [26], which is based on the Heisenberg–Langevin equations of motion for the atomic and field operators. The Hamiltonian of the system in the rotating wave approximation can be written in the form:

$$\begin{aligned} H = -\hbar[&\Omega_{32}\sigma_{32}\, e^{-i\omega t} + \Omega_{41}\sigma_{41}\, e^{-i\omega t} \\ &+ \Omega_{31}\sigma_{31}\, e^{-i\omega t} + \Omega_{42}\sigma_{42}\, e^{-i\omega t} \\ &+ g_{31}\sigma_{31}a + g_{42}\sigma_{42}a + g_{31}\sigma_{31}b + g_{42}\sigma_{42}b \\ &+ g_{32}\sigma_{32}a + g_{41}\sigma_{41}a + g_{32}\sigma_{32}b + g_{41}\sigma_{41}b] \\ &+ \text{H.c.}, \end{aligned} \tag{1}$$

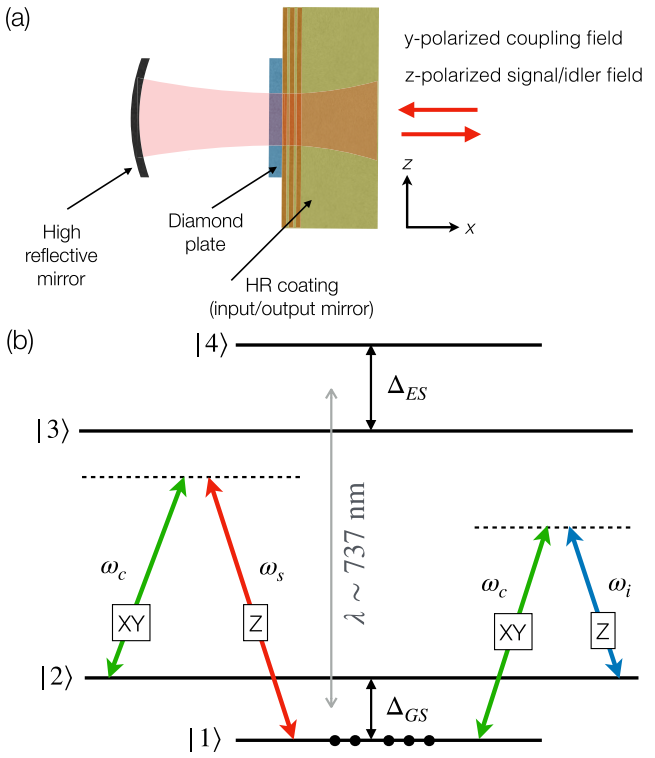

Figure 1. Schematic diagram of the cavity-based Raman quantum memory (a) and energy level diagram (b).

where $a = A\exp(-i\omega_s t)$ and $b = B\exp(-i\omega_i t)$ are the annihilation operators for the photons of the signal and idler fields, respectively, in the resonator modes; $\sigma_{mn} = P_{mn}\exp(i\omega_{mn}t)$ are the atomic transition operators ($\sigma_{mn} = |m\rangle\langle n|$, $m, n = \{1, 2, 3, 4\}$); and A, B and P_{mn} are slowly varying field and coherence amplitudes, respectively. The frequencies ω_{mn} are taken as follows: $\omega_{31} = \omega_{41} = \omega_s$, $\omega_{32} = \omega_{42} = \omega$, $\omega_{21} = \omega_s - \omega$ (other frequencies are not relevant in the present model). For an ensemble of $N \gg 1$ optical centers, taking into account that in the process of interaction with a weak signal field almost all centers remain in the ground state ($\langle\sigma_{11}\rangle \approx N$, $\langle\sigma_{22}\rangle \approx \langle\sigma_{33}\rangle \approx \langle\sigma_{44}\rangle \approx 0$), from the Heisenberg–Langevin equations we obtain:

$$\begin{aligned} \dot{P}_{12} = &-\gamma_{12}P_{12} - i\Delta_{12}P_{12} + i\Omega_{32}^{*}P_{13} + i\Omega_{42}^{*}P_{14} \\ &- i\Omega_{41}P_{42}\, e^{-i\delta t} - i\Omega_{31}P_{32}\, e^{-i\delta t} \\ &- ig_{31}P_{32}A\, e^{i2\delta t} - ig_{31}P_{32}B\, e^{i(\delta'+\delta)t} \\ &+ ig_{42}^{*}P_{14}A^{\dagger}\, e^{-i\delta t} + ig_{42}^{*}P_{14}B^{\dagger}\, e^{-i\delta' t} \\ &- ig_{41}P_{42}A - ig_{41}P_{42}B\, e^{i(\delta'-\delta)t} \\ &+ ig_{32}^{*}P_{13}A^{\dagger}\, e^{-i\delta t} + ig_{32}^{*}P_{13}B^{\dagger}\, e^{-i\delta' t}, \end{aligned} \tag{2}$$

$$\begin{aligned} \dot{P}_{13} = &-\gamma_{13}P_{13} - i\Delta_{13}P_{13} + i\Omega_{32}P_{12} + i\Omega_{31}\sqrt{N}\, e^{-i\delta t} \\ &+ ig_{31}\sqrt{N}A + ig_{31}\sqrt{N}B\, e^{i(\delta'-\delta)t} \\ &+ ig_{32}P_{12}A\, e^{i\delta t} + ig_{32}P_{12}B\, e^{i\delta' t}, \end{aligned} \tag{3}$$

$$\begin{aligned} \dot{P}_{23} = &-\gamma_{23}P_{23} - i(\Delta_{13} - \Delta_{12})P_{23} + i\Omega_{31}P_{21}\, e^{-i\delta t} \\ &+ ig_{31}P_{21}A + ig_{31}P_{21}B\, e^{i(\delta'-\delta)t}, \end{aligned} \tag{4}$$

$$\dot{P}_{14} = -\gamma_{14}P_{14} - i\Delta_{14}P_{14} + i\Omega_{42}P_{12} + i\Omega_{41}\sqrt{N}\,e^{-i\delta t} + ig_{41}\sqrt{N}A + ig_{41}\sqrt{N}B\,e^{i(\delta'-\delta)t} + ig_{42}P_{12}A\,e^{i\delta t} + ig_{42}P_{12}B\,e^{i\delta' t}, \quad (5)$$

$$\dot{P}_{24} = -\gamma_{24}P_{24} - i(\Delta_{14}-\Delta_{12})P_{24} + i\Omega_{41}P_{21}\,e^{-i\delta t} - ig_{41}P_{21}A - ig_{41}P_{21}B\,e^{i(\delta'-\delta)t}, \quad (6)$$

$$\dot{A} = -\kappa A + \sqrt{2\kappa}A_{in} + ig_{31}^{*}P_{13} + ig_{41}^{*}P_{14} + ig_{32}^{*}P_{23}\,e^{-i\delta t} + ig_{42}^{*}P_{24}\,e^{-i\delta t}, \quad (7)$$

$$\dot{B} = -\kappa B + \sqrt{2\kappa}B_{in} + ig_{31}^{*}P_{13}\,e^{i(\delta-\delta')t} + ig_{41}^{*}P_{14}\,e^{i(\delta-\delta')t} + ig_{32}^{*}P_{23}\,e^{-i\delta' t} + ig_{42}^{*}P_{24}\,e^{-i\delta' t}, \quad (8)$$

where $\delta = \omega - \omega_s$, $\delta' = \omega - \omega_i$, $\Delta_{13} = \omega_{33} - \omega_s$ is the one-photon detuning ($\Delta_{14} = \Delta_{13} + \Delta_{ES}$), $\Delta_{12} = \omega_{22} + \omega - \omega_s$ is the two-photon detuning ($\hbar\omega_{nn}$ corresponds to the energy of the nth level relative to the ground one), $g_{mn} = d_{mn}\sqrt{\omega/(2\hbar\varepsilon_0 V)}$ is the coupling constant between the field and optical centers at the $|m\rangle - |n\rangle$ transition, which is characterised by the dipole moment d_{mn}; γ_{mn} are the decay rates of coherences; 2κ is the decay rate of the resonator field, and V is the volume of the resonator field mode. The collective atomic operators are normalized as follows: $P_{mn} = \sum_{j=1}^{N} P_j/\sqrt{N}$. In the case of an exact two-photon resonance, when $\Delta_{12} = 0$, we have $\delta = -\delta'$, so that $|\delta|$ is equal to the frequency separation Δ_{GS} between the states $|1\rangle$ and $|2\rangle$. In doing so, the two-photon detuning Δ_{12} is modulated in time to take into account the two-photon frequency shift induced by the time-dependent control field, which is equal to $-|\Omega_{32}|^2/\Delta_{13}$ in a simple three-level case, but corrected numerically in the present model (by a multiplier) to maximize the quantum memory efficiency.

In possession of a solution for the resonator field amplitude $A(t)$ we can find the amplitude of the signal field at the output of the resonator $A_{out}(t)$ from the boundary condition $A_{out}(t) = \sqrt{2\kappa}A(t) - A_{in}(t)$. For the system of equations (2)–(8) to be solved numerically, the operators are replaced by complex numbers corresponding to the amplitudes of the transition probability between the vacuum and single-photon states for the field and between the ground and excited states for optical centers. In doing so, the input idler field B_{in} is assumed to be zero. Since almost all optical centers are in the ground state, the contribution of atomic noise operators in the Heisenberg–Langevin equations can be neglected so that they are not included in the system of equations.

The relative dipole moments of the optical transitions for the SiV centers are calculated using eigenstates of the total Hamiltonian [23] with strain susceptibility parameters from [27]. To be more specific, we consider so-called E_g-strain that leads to a larger frequency splitting between the sublevels of the ground state. It turns out that the larger the strain, the weaker the coupling of the y-polarized control field to the unwanted transition $|1\rangle - |3\rangle$, i.e. the weaker the noise. Table 1 illustrates the relative probabilities of the optical transitions calculated for the case of high E_g-strain ($1.7 \cdot 10^{-4}$), when $\Delta_{GS} = 463$ GHz and $\Delta_{ES} = 698$ GHz. This case is taken for quantum memory simulation below. The dipole moment for the transition $|1\rangle - |3\rangle$ and z-polarized light (signal field) is estimated as 14.3 D [5].

Table 1. Relative transition intensities $|g_{mn}/g_{13}|^2$ for coupling to an z-polarized (y-polarized) light under conditions of zero strain (above) and E_g-strain of $1.7 \cdot 10^{-4}$ (below).

	$\|3\rangle$	$\|4\rangle$
$\|1\rangle$	1 (0.0251)	0.0378 (0.2343)
$\|2\rangle$	0.0378 (0.2343)	1 (0.0251)
	$\|3\rangle$	$\|4\rangle$
$\|1\rangle$	1 (0.0057)	0.0206 (0.2494)
$\|2\rangle$	0.0206 (0.2494)	1 (0.0057)

4. Simulation results

The quantum memory is basically characterized by the total efficiency, which is defined as

$$\eta = \frac{\int |A_{out}(t)|^2\,dt}{\int |A_{in}(t)|^2\,dt}, \quad (9)$$

where $A_{in}(t)$ and $A_{out}(t)$ are the amplitudes of the input and output pulses, respectively, well separated in time. For the high efficiency to be achieved, the time dependence of the control field during storage (via off-resonant Raman absorption) and retrieval (via off-resonant Raman scattering) should be optimized for given input and output pulse shapes [28]. In this case, the efficiency is limited basically by coherence decay during storage time. Another important parameter describing the quantum memory scheme is the noise that appears during retrieval, which is defined as radiation at the signal field frequency that arises when the control field is applied to the atomic ensemble (during both storage and retrieval slots) in the absence of an input pulse. In general, at the output of the device one observes the sum of the useful signal and the noise, which is characterised by the signal-to-noise ratio

$$\mathrm{SNR} = \left(\frac{\int |A_{noise}|^2\,dt}{\int |A_{out}|^2\,dt}\right)^{-1}. \quad (10)$$

In what follows, we consider storage and retrieval of Gaussian single-photon pulses with the amplitude

$$A_{in} = A_{in}^{0}\exp[-R(t-T)^2], \quad (11)$$

where $\int |A_{in}|^2\,dt = 1$ is the normalisation corresponding the the single-photon state and the parameter R is related to the pulse duration (FWHM) $\tau = \sqrt{2\ln 2}/R$. The optimal time dependence of the Rabi frequency $\Omega_{32}(t)$ during storage and retrieval, which results in the emission of a Gaussian pulse, can be described analytically [26].

To be more specific, we consider a semiconfocal microresonator of $\sim$50 μm in length with the input/output mirror

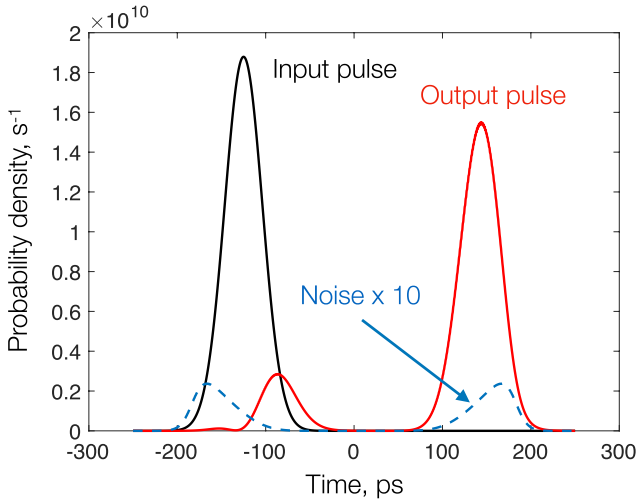

Figure 2. Illustrating storage and retrieval of single-photon Gaussian pulses in an ensemble of SiV centers. The result of numerical solution of equations (2)–(8) for $\tau = 50$ ps, $\Delta_{13}/2\pi = 200$ GHz, $N = 2600$, $\kappa/2\pi = 9$ GHz, peak value of $\Omega_{32}/2\pi = 80$ GHz, $\gamma_{13}/2\pi = \gamma_{14}/2\pi = \gamma_{23}/2\pi = \gamma_{24}/2\pi = 130$ MHz, $\gamma_{12}/2\pi = 6$ MHz, $|\delta|/2\pi = |\delta'|/2\pi = 463$ MHz, $g_{13}/2\pi = 396$ MHz.

reflectivity of 0.97. The latter corresponds to the cavity finesse of about 200, which provides the cavity linewidth of 18 GHz allowing storage of pulses as short as 50 ps. A thin (1 μm) diamond plate is located at the focal plane where the beam spot is of $\sim$4 μm in diameter. An example of such a resonator system has been recently demonstrated in [7]. Then, according to the numerical simulation, we can obtain SNR $\approx$ 50 at the output of the memory for Gaussian single-photon pulses of 50 ps duration, which strongly depends on the number of color centers, control field intensity and one-photon detuning. This can be understood by considering far-off-resonant interaction, when the optical coherences can be adiabatically eliminated from the equations of motion, which gives $dP_{12}/dt = \ldots + \Omega_{32}^{*}\Omega_{31}\sqrt{N}\exp(-i\delta t)/\Delta_{13} + \Omega_{42}^{*}\Omega_{41}\sqrt{N}\exp(-i\delta t)/\Delta_{14}$. It is these terms on the right side of the equation that are responsible for noise in the present model. They appear only due to coupling of the control field to the unwanted optical transitions $|1\rangle - |3\rangle$ and $|1\rangle - |4\rangle$, which is reduced with strain. Figure 2 displays the result of simulation for such pulses interacting with 2600 SiV centers in the sample subjected by high E_g-strain mentioned above. The total efficiency is about 90% (for the time-bandwidth product of 6 and coherence time of 35 ns) provided that inhomogeneous broadening of the low frequency transition $|1\rangle - |2\rangle$ is reversed at the moment of time $t = 0$. Otherwise, the total efficiency drops to 29% for the inhomogeneous broadening of 350 MHz. The latter can be expected taking into account the minimum values observed for the optical transitions [29]. Similar results of simulation are obtained for longer pulses. In this case, noise is smaller because longer pulses require smaller intensity of the control field and smaller number of color centers. In particular, for 100 ps pulses we obtain SNR $\approx$ 230 taking one-photon detuning of 100 GHz, peak value of the Rabi frequency $\Omega_{13}/2\pi = 40$ GHz and the number of color centers of about 1500.

5. Conclusion

In summary, we have developed a theoretical model describing the storage and retrieval of weak light pulses via off-resonant Raman absorption and emission of photons in an ensemble of four-level optical centers that have nonorthogonally polarized optical transitions. Using this model, we have analyzed the signal-to-noise ratio at the output of an optical quantum memory device based on an ensemble of SiV centers in diamond. The numerical results show that the signal-to-noise ratio can significantly exceed unity for short single-photon input pulses if the number of optical centers is small enough, and level splitting in their ground state is significantly enhanced by strain.

Acknowledgments

AK, AB and PH acknowledge financial support from the Government of the Russian Federation (Mega-Grant No. 14.W03.31.0028). OK acknowledges support from National Science Foundation (Grant No. PHY 1820930 and Grant No. PHY 150-64-67). AK and OK deeply acknowledge many years of fruitful scientific interaction with Professor Samartsev. His work on coherent effects in optical centers in solids and his unique personality have been always inspiring for us.

References

[1] Bussières F, Sangouard N, Afzelius M, de Riedmatten H, Simon C and Tittel W 2013 *J. Mod. Opt.* **60** 1519–37
[2] Heshami K, England D G, Humphreys P C, Bustard P J, Acosta V M, Nunn J and Sussman B J 2016 *J. Mod. Opt.* **63** 2005–28
[3] Awschalom D D, Hanson R, Wrachtrup J and Zhou B B 2018 *Nat. Photon.* **12** 516–27
[4] Atatüre M, Englund D, Vamivakas N, Lee S Y and Wrachtrup J 2018 *Nat. Rev. Mater.* **3** 38–51
[5] Becker J N and Becher C 2017 *Phys. Status Solidi* a **214** 1700586
[6] Zhang J L *et al* 2017 *Optica* **4** 1317–21
[7] Sukachev D D, Sipahigil A, Nguyen C T, Bhaskar M K, Evans R E, Jelezko F and Lukin M D 2017 *Phys. Rev. Lett.* **119** 223602
[8] Becker J N, Pingault B, Groß D, Gündoğan M, Kukharchyk N, Markham M, Edmonds A, Atatüre M, Bushev P and Becher C 2018 *Phys. Rev. Lett.* **120** 053603
[9] Sun S *et al* 2018 *Phys. Rev. Lett.* **121** 083601
[10] Weinzetl C, Görlitz J, Becker J N, Walmsley I A, Poem E, Nunn J and Becher C 2019 *Phys. Rev. Lett.* **122** 063601
[11] Häußler S, Benedikter J, Bray K, Regan B, Dietrich A, Twamley J, Aharonovich I, Hunger D and Kubanek A 2019 *Phys. Rev.* B **99** 165310
[12] Nunn J, Walmsley I A, Raymer M G, Surmacz K, Waldermann F C, Wang Z and Jaksch D 2007 *Phys. Rev.* A **75** 011401
[13] Reim K F, Nunn J, Jin X M, Michelberger P S, Champion T F M, England D G, Lee K C, Kolthammer W S, Langford N K and Walmsley I A 2012 *Phys. Rev. Lett.* **108** 263602
[14] Moiseev S A and Tittel W 2011 *New J. Phys.* **13** 063035
[15] Moiseev S A 2013 *Phys. Rev.* A **88** 012304

[16] Zhang X, Kalachev A and Kocharovskaya O 2013 *Phys. Rev.* A **87** 013811
[17] Kalachev A and Kocharovskaya O 2013 *Phys. Rev.* A **88** 033846
[18] Zhang X, Kalachev A and Kocharovskaya O 2014 *Phys. Rev.* A **90** 052322
[19] Zhang X W, Kalachev A, Hemmer P, Scully M O and Kocharovskaya O 2014 *Laser Phys.* **24** 094016
[20] Zhang X, Kalachev A, Hemmer P and Kocharovskaya O 2016 (arXiv:1602.02322 [quant-ph])
[21] Heshami K, Santori C, Khanaliloo B, Healey C, Acosta V M, Barclay P E and Simon C 2014 *Phys. Rev.* A **89** 040301
[22] Nunn J *et al* 2017 *Phys. Rev.* A **96** 012338
[23] Hepp C *et al* 2014 *Phys. Rev. Lett.* **112** 036405
[24] Pingault B, Becker J N, Schulte C H H, Arend C, Hepp C, Godde T, Tartakovskii A I, Markham M, Becher C and Atatüre M 2014 *Phys. Rev. Lett.* **113** 263601
[25] Sohn Y I *et al* 2018 *Nat. Commun.* **9** 2012
[26] Berezhnoi A D and Kalachev A A 2017 *Quantum Electron.* **47** 790–3
[27] Meesala S *et al* 2018 *Phys. Rev.* B **97** 205444
[28] Gorshkov A V, André A, Lukin M D and Sørensen A S 2007 *Phys. Rev.* A **76** 033804
[29] Sipahigil A, Jahnke K D, Rogers L J, Teraji T, Isoya J, Zibrov A S, Jelezko F and Lukin M D 2014 *Phys. Rev. Lett.* **113** 113602